Non-Newtonian 3d Ciliary Fluid Flow in a Semi-Infinite Domain

Dragos Isvoranu*, Sterian Danaila

* Corresponding author: Tel.: ++40 (0) 21 3250704; Email: ddisvoranu@gmail.com
Fac. of Aerospace Engineering, University Politehnica of Bucharest, RO

Abstract Continuing our previous investigations in ciliary fluid transportation (Isvoranu et al., 2010) our present paper looks into the matter of non-newtonian fluid flow. Naturally, in constant properties fluids (newtonian fluids) ciliary transportation is based on a non-symmetric actuation mechanism meaning different geometrical configuration of the cilium during the active and passive stroke. Artificial cilia can mimick this behaviour through asymmetric magnetic actuation as discused in (Isvoranu et. al., 2008). What happens when fluid properties (eg. viscosity) are not constant throughout a beating cycle? Such situation is expected to be encountered when dealing with biological fluids like saliva, for example. In the case of a shear-thinning fluid, like the above mentioned one, the motion can also become asymetric due to deformation rate dependent viscosity that ultimately leads to different time scales of the forward and backward strokes. In the present paper we are investigating a 3D flow generated by an array of cilia embedded in a non-newtonian fluid whose viscosity is characterized by a power low shear rate dependency. The same magnetic actuation mechanism is considered.

Keywords: Micro Flow, Magnetic Actuation

1. Introduction

In present, the possibilities to manipulate fluids at the micro or nano scales is investigated by many researchers. The envisaged applications, imposed by future high-tech technology, are inkjet printing for displays, micro-channel cooling for electronics and biomedical applications (controlled drug delivery systems, biosensors). Considering the various applications, the fluids to be manipulated are no longer Newtonian (polymer solutions, blood, saliva, urine). Knowing that the typical sizes of the micro-fluid channel widths and heights range from several to hundreds of micrometers, the manipulation mechanism may be quite different: transportation, mixing, sorting, deforming, or rupturing. However, we emphasize the "designed" by nature manipulation that is that due to a covering of beating cilia over the external surface of micro-organisms (e.g. paramecium, pleurobrachia, and opaline). A cilium is similar to a small wire or flexible rod (in protozoa: typical length 10 mm and diameter 0.1 mm) attached to the surface. The cilia, collectively and correlated move forth and back, and in this way generate flow (for example, the propulsion speed produced by paramecium cilia is in the order of several mm/s). The induced flow by the artificial cilia has several distinctive particularities comparing to the biological counterpart. The main dissimilarity is the different way of attaching the cilium to the support substrate and problem of mimicking the difference between cilium's inner engine behavior during the active and passive stroke.

Initially, the adopted physical flow models were based on downscaling of existing flow models in regular devices, such as pumps, valves, or mixers. Further, the flow models take into account the nonnegligible small scales effects, such as surface tension, surface energy patterning, or electro-osmosis.

In the present paper we are investigating a 3D flow generated by an array of cilia embedded in a non-Newtonian fluid whose viscosity is characterized by a power low shear rate dependency. The actuation mechanism considered is magnetic.

2. Structural model

The cilium is modeled as an inextensible, but deformable, cylindrical filament with circular cross section of constant radius *a*. The geometry is defined in some fixed Cartesian coordinate system (x, y, z). We assume the slenderness $\varepsilon = a/L << 1$, where L is the constant length of the cilium. If we assume that the cross section remains always planar, the deformed geometry can be recovered from three sets of data: the position of points lying on filament centreline, the twisting and the rotation of cross sections passing through these points. The points on the filament centreline are defined by the position vector $\boldsymbol{r}(s,t) = \big(x(s,t), y(s,t), z(s,t)\big)$ where s $(0 \le s \le L)$ is its arc-length and t time. We assume $s = 0$ for the anchor point and $s = L$ at the distal end point. Lets' be $A(s,t)$ an arbitrary point along the centreline curve and $\Pi(s,t)$ the normal to the centre line plane passing through the point $A(s,t)$ plane. Following (Gueron and Levit-Gurevich, 2001) at each point along the curve we define an local orthonormal coordinate system by the three unit vectors $\boldsymbol{X} = \boldsymbol{X}(s,t)$, $\boldsymbol{Y} = \boldsymbol{Y}(s,t)$ $\boldsymbol{Z} = \boldsymbol{Z}(s,t)$ such that vector $\boldsymbol{Z}$ points in the direction of the tangent to the centreline. This Lagrangian coordinate system (body-coordinate system (Hines and Blum, 1978)) offers the possibility of constructing a reliable model for the dynamics of an inextensible filament avoiding the undesired singularity stemming from inextensibility condition associated with Serret-Frenet formulation of the former model of Gueron and Liron (Gueron and Liron, 1992). Vector $\boldsymbol{X}$ can be chosen arbitrarily under the condition that for the straight and untwisted filament all corresponding vectors for $0 \le s \le L$ are parallel and point in the same direction. The third unit vector $\boldsymbol{Y}$ is determined from the requirement that $\boldsymbol{Y} = \boldsymbol{Z} \times \boldsymbol{X}$. An illustration of this coordinate system is provided in Fig. 1. For dynamic problems, the cross section defined by $(\boldsymbol{X}, \boldsymbol{Y})$ plane may also rotate along $\boldsymbol{Z}(s,t)$ axis at an angular velocity $\boldsymbol{\Omega}(s,t) = \Omega(s,t)\boldsymbol{Z}(s,t)$.

The link between fixed and body coordinate systems is done by the Euler rotation matrices, $\boldsymbol{R}_X(\varphi)$, $\boldsymbol{R}_Y(\theta)$, $\boldsymbol{R}_Z(\psi)$ as follows:

$$\begin{bmatrix} x \\ y \\ z \end{bmatrix} = \boldsymbol{R}_X(\varphi)\boldsymbol{R}_Y(\theta)\boldsymbol{R}_Z(\psi)\begin{bmatrix} X \\ Y \\ Z \end{bmatrix}$$
$$\begin{bmatrix} X \\ Y \\ Z \end{bmatrix} = \boldsymbol{R}_Z(\psi)\boldsymbol{R}_Y(\theta)\boldsymbol{R}_X(\varphi)\begin{bmatrix} x \\ y \\ z \end{bmatrix} \quad (1)$$

where angles φ, θ and ψ are three successive rotations.

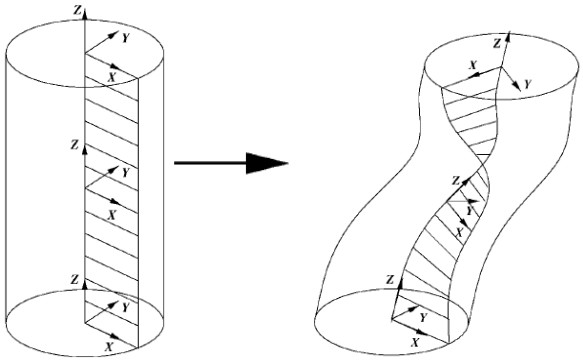

Figure 1. Body coordinate system of a cylindrical filament.

We define $k_X = k_X(s,t)$, $k_Y = k_Y(s,t)$ and $k_Z = k_Z(s,t)$, the infinitesimal changes of body coordinates from s to the ones at $s + ds$ through:

$$k_X = \frac{\partial\varphi}{\partial s}, k_Y = \frac{\partial\theta}{\partial s}, k_Z = \frac{\partial\psi}{\partial s} \quad (2)$$

We note that k_X, k_Y and k_Z are related to the rates of change of unit vectors $\boldsymbol{X} = \boldsymbol{X}(s,t)$, $\boldsymbol{Y} = \boldsymbol{Y}(s,t)$, $\boldsymbol{Z} = \boldsymbol{Z}(s,t)$ as a function of *s*:

$$\frac{d\boldsymbol{X}}{ds} = k_Z\boldsymbol{Y} - k_Y\boldsymbol{Z}, \frac{d\boldsymbol{X}}{ds} = k_Z\boldsymbol{Y} - k_Y\boldsymbol{Z},$$
$$\frac{d\boldsymbol{Z}}{ds} = k_Y\boldsymbol{X} - k_X\boldsymbol{Y} \quad (3)$$

The rates of change of unit vectors $\boldsymbol{X} = \boldsymbol{X}(s,t)$, $\boldsymbol{Y} = \boldsymbol{Y}(s,t)$, $\boldsymbol{Z} = \boldsymbol{Z}(s,t)$ as a function of t are denoted as $\omega_X = \omega_X(s,t)$, $\omega_Y = \omega_Y(s,t)$ and $\omega_Z = \omega_Z(s,t)$. We mention that $\omega_Z(s,t) \neq \Omega(s,t)$. Obviously:

$$\frac{\partial\boldsymbol{u}}{\partial s} = \left(\frac{\partial\boldsymbol{u}}{\partial s}\right)_{body} + \boldsymbol{k} \times \boldsymbol{u},$$
$$\frac{\partial\boldsymbol{u}}{\partial t} = \left(\frac{\partial\boldsymbol{u}}{\partial t}\right)_{body} + \boldsymbol{\omega} \times \boldsymbol{u} \quad (4)$$

where subscript $_{body}$ refers to representation of arbitrary vector with respect to body coordinates system. The time evolution of the curve expressed in body coordinates is

described by the following set of equations (Gueron and Levit-Gurevich, 2001):

$$\dot{k}_X = k_Y\omega_Z - \boldsymbol{V}_{ss}\cdot\boldsymbol{Y} \quad (5)$$

$$\dot{k}_Y = -k_X\omega_Z + \boldsymbol{V}_{ss}\cdot\boldsymbol{X} \quad (6)$$

$$\dot{k}_Z = \omega_{Z_s} + k_X\boldsymbol{V}_s\cdot\boldsymbol{X} + k_Y\boldsymbol{V}_s\cdot\boldsymbol{Y} \quad (7)$$

$$\omega_{Z_s} = \Omega_s - k_X\boldsymbol{V}_s\cdot\boldsymbol{X} - k_Y\boldsymbol{V}_s\cdot\boldsymbol{Y} \quad (8)$$

where $\boldsymbol{V} = \boldsymbol{V}(s,t)$ is the velocity of the filament. For simplicity, we use subscripts subscript $_s$ to denote differentiation with respect to the arc-length s and superscript $\dot{}$ to denote differentiation with respect to time. The above differential system allows to determine k_X, k_Y, k_Z and twisting rate ω_Z when $\boldsymbol{V}$ and Ω are done. The inextensibility condition $\boldsymbol{Z}\cdot\boldsymbol{V} = 0$ yields

$$V_{Z_s} - k_Y\boldsymbol{V}_X + k_X\boldsymbol{V}_Y = 0 \quad (9)$$

Knowing the anchor location $\boldsymbol{r}(s_0,t)$ and orientation $\boldsymbol{X}(s_0,t)$, $\boldsymbol{Y}(s_0,t)$, $\boldsymbol{Z}(s_0,t)$ the reconstruction of the cilium centreline with respect to the fixed coordinate system is provided by the following integral

$$\boldsymbol{r}(s,t) = \boldsymbol{r}(0,t) + \int_0^s \boldsymbol{Z}(\xi,t)d\xi \quad (10)$$

Integration of the differential system (3) provides the unit vectors necessary in the reconstruction process. Rotation angles $\varphi = \varphi(s,t)$, $\theta = \theta(s,t)$ and $\psi = \psi(s,t)$ are computed by integrating Eq. (2) with appropriate initial conditions.

3. Dynamic model

The mechanical equilibrium expresses the balance of forces and moments acting of each individual cilium (Gueron and Liron, 1992; Gueron et.al, 1997; Gueron et.al., 1998; Gueron and Liron., 1999):

$$\boldsymbol{\phi} = \boldsymbol{F}_s, \boldsymbol{F} = \boldsymbol{M}_{e,s} + \boldsymbol{T}_s \quad (11)$$

unde $\boldsymbol{\phi} = \boldsymbol{\phi}(s,t)$ este is the viscous forces per unit length (drag forces) exerted by the surrounding fluid, $\boldsymbol{T} = \boldsymbol{T}(s,t)$ is the driving engine is represented by the magnetic torque exerted on each cilia, $\boldsymbol{F} = \boldsymbol{F}(s,t)$ is the shear force, $\boldsymbol{M}_e = \boldsymbol{M}_e(s,t)$ is the elastic torque. In the local coordinate system Eqs. 11 become:

$$\phi_X = F_{X,s} - k_Z F_Y + k_Y F_Z$$
$$\phi_Y = F_{Y,s} + k_Z F_X - k_X F_Z$$
$$\phi_Z = F_{Z,s} - k_Y F_X + k_X F_Y$$

$$F_X = E_B k_{Y,s} + (E_B - E_T)k_X k_Z + S$$
$$F_Y = -E_B k_{X,s} + (E_B - E_T)k_Y k_Z + P \quad (12)$$

where E_B and E_T represent cilium elastic moduli to bending and twisting and the components of the derivative of the magnetic torque are denoted by $S^{(k)}$ and $P^{(k)}$.

$$S = T_{Y,s} + k_Z T_X - k_X T_Z$$
$$P = -T_{X,s} + k_Z T_Y - k_Y T_Z \quad (13)$$

The asymptotic relation between drag forces and velocity derived by Gueron and Liron (Gueron and Levit-Gurevich, 1992) provides the link between dynamics and kinematics of the cilia 9 pt Times New Roman font.

$$\phi_X = -C_X V_X + g_X$$
$$\phi_Y = -C_Y V_Y + g_Y$$
$$\phi_Z = -C_Z V_Z + g_Z \quad (14)$$

where $g_X = C_X G_X$, $g_Y = C_Y G_Y$, $g_Z = C_Z G_Z$ and the drag coefficients are given by

$$C_Z = \frac{8\pi\mu}{-2 + 4ln(2q/a)}$$
$$C_X = C_Y = \frac{8\pi\mu}{1 + 2ln(2q/a)} \quad (15)$$

μ being the molecular viscosity. For non-Newtonian fluids, μ is not longer constant and have to be considered as variable in s direction, $\mu = \mu(s)$. The vector $\boldsymbol{G} = (G_X, G_Y, G_Z)$ denotes the velocity field induced at s by far segments of the cilium and neighbouring cilia. The components of $\boldsymbol{G}$ are integrals of the appropriate fundamental solutions of the Stokes equations and are expressed by:

$$\boldsymbol{G}(s_0,t) = \int_{|s-s_0|>q}^{L} \boldsymbol{U}_{Stoklet}(\boldsymbol{r},\boldsymbol{r}_0,-\boldsymbol{\phi})ds$$
$$+ \int_0^L \{\boldsymbol{U}_{Image\ system}(\boldsymbol{r},\boldsymbol{r}_0,-\boldsymbol{\phi}) \quad (16)$$
$$+ \boldsymbol{U}_{Doublet\ image\ system}(\boldsymbol{r},\boldsymbol{r}_0,-\boldsymbol{\phi}a^2/4\mu)\}ds$$

for any q such that $a \ll q$ and $q \ll L$ (in present work we used $q = 0.1L$). The viscous torque per unit length exerted on a rotating cylinder in Stokes flow can be approximated by a linear function of its angular velocity Ω. Following (Gueron and Levit-Gurevich, 2001) we find

$$\Omega = \frac{E_T}{C_\Omega}k_{Z,s} + \frac{R}{C_\Omega} \quad (17)$$

where $R = R(s,t)$ is the active twisting moment per unit length and $C_\Omega = 4\pi\mu a^2$ is

the resistance coefficient. The magnetic actuation is produced by a rotating magnetic field generated with either longitudinal or longitudinal and transversal coils. Harmonic excitation of coils is assumed. In the present paper the cilium is considered being made of a permanently magnetic material with saturation magnetization (PMM). The magnetic torque per control volume for a constant longitudinal saturation magnetization in the body coordinate system is simply (Jackson, 1974)

$$(d\boldsymbol{T})_{body} = \frac{\left(\boldsymbol{M}_{sat} \times \boldsymbol{B}_{body}\right)\pi a^2 ds}{4} \quad (18)$$

4. Constitutive relations

Constitutive relations express the stress components in terms of the primary unknowns (more exactly, in terms of strain or rate of strain). In the case of a fluid at rest, the stress is determined wholly by the one scalar quantity *p*, the static-fluid pressure, and *p* in turn is specified locally by the equilibrium equation of state when the values of the two parameters of state (e.g. density and temperature) are known. In the case of a fluid in relative motion, the connection between the stress and the local properties must account for all events during the motion of fluid particles that contribute to the local stress (Bird et al. 1987). The constitutive relations are more complicated, in two respects: first, the stress tensor contains a non-isotropic part as well as an isotropic part, and second, the scalar quantity *p* specifying the isotropic part is not itself one of the variables of state used in equilibrium thermodynamics. The first of these two manifestations of the departure from equilibrium represents a transport of momentum, or internal friction, and is by far the more important, in the great majority of flow fields (Batchelor , 1967).

A non-Newtonian fluid is one whose stresses are not linear with the rate of strain, but is dependent on flow conditions such as flow geometry, shear rate, etc. and sometimes even on the kinematic history of the fluid element under consideration. Such materials (i.e. fluids of elaborate molecular structure, and in particular for those consisting of long molecular chains, and for some emulsions and mixtures) may be conveniently grouped into three general classes (Astarita et al., 1977, Chhabra et. al, 1999):

1. Fluids for which the rate of shear at any point is determined only by the value of the shear stress at that point at that instant; these fluids are variously known as “time independent” or “generalised Newtonian fluids”;
2. Fluids for which the relation between shear stress and shear rate depends, in addition, upon the duration of shearing and their kinematic history; they are called “time-dependent fluid”;
3. Fluids exhibiting characteristics of both ideal fluids and elastic solids and showing partial elastic recovery, after deformation; these are categorized as “visco-elastic fluids”.

This classification scheme is arbitrary in that most real materials often exhibit a combination of two or even all three types of non-Newtonian features. Generally, it is, however, possible to identify the dominant non-Newtonian characteristic and to take this as the basis for the subsequent process calculations.

For non-Newtonian fluids the stresses linear dependence of rate of strain cease to be accurate at only moderate rates of strain; the stress depends on the strain history as well as on its instantaneous rate of change. The measurable effects of these historical events can be quantified, for example, by the Rivlin-Ericksen strain tensors (Malvern, 1969). In our specific case, we chose to simulate the behaviour of the cilium in a visco-elastic environment like shear-thinning fluid. In this case, $\mu = m\dot{\gamma}^{n-1}$ where $n < 1$ and $\dot{\gamma}$ is the second invariant of the strain rate tensor, $\dot{\gamma}^2 = 0.5\dot{\gamma}_{ij}\dot{\gamma}_{ij}$, $\dot{\gamma}_{ij} = u_{i,j} + u_{j,i}$represents the so called power law model. There are various alternatives of this basic generalization of the Newtonian fluids, among which we recall the Casson and Quemada models. These last models extends the range of aplicability of the power-law model and improve its convergence properties to the Newtonian limit. Human saliva is one typical shear-thinning fluid whose molecular viscosity, based on rheological measurements, can be fitted to the formula

$$\mu(\dot{\gamma}) = \mu_\infty + \frac{\mu_0 - \mu_\infty}{[1 + (\tau\dot{\gamma})^2]^{0.4}} \qquad (19)$$

where $\mu_0 = 70$ Pa·s, $\mu_\infty = 0.001$ Pa·s and $\tau = 100$ s (Balthussen et al., 2010).

5. Dimensionless equations

We define the dimensionless quantities:

$$\bar{F} = \frac{F}{S_0}, \bar{s} = \frac{s}{L}, \bar{g} = \frac{gL}{S_0}, \bar{\phi} = \frac{\phi L}{S_0},$$

$$\bar{t} = ft, \bar{k} = kL, \bar{E}_B = \frac{E_B}{S_0 L^2}$$

$$\bar{C}_X = \frac{C_X L^2 f}{S_0}, \bar{C}_Z = \frac{C_Z L^2 f}{S_0}, \bar{C}_\Omega = \frac{C_\Omega f}{S_0}.$$

where S_0 and $1/f$ are the force scale and time scale, respectively. The last three quantities vary liniary with molecular viscosity along cilium length. Using equations (12)-(17) and (5) the differential equation for F_Z is obtained. Extracting the components of the velocity field from Eq. (11) and inserting them into kinematic conditions (4)-(7) we obtain the complete set of equations for simulating the 3D ciliary motion. However, due to restricted space and their length, we refer the reader to (Isvoranu et al., 2010) in order to catch a glimpse of their bulkiness, not to mention the extra terms generated by the new viscosity variable. From the numerical point of view, the centreline is discretized in *N*+1 equally spaced grid points, spatial derivatives are replaced by time averaged central finite differences while the temporal derivatives by a forward in time difference. This approach leads to a more stable Cranck-Nicholson numerical scheme. Larger time steps are easily attainable. However, due to the high nonlinearity of the equations the solution algorithm must proceed iteratively with two inner loops of refinement for the fundamental solutions and k_X, k_Y, k_Z and ω_Z and an outer loop for viscosity and implicitely for the drag coefficients $\bar{C}_X$, $\bar{C}_Z$ and $\bar{C}_\Omega$.

6. Results

A computer code has been devised in order to perform the necessary simulations. All external inputs and other parameters range of variation have been imposed such that to ensure mechanical and geometrical stability. Their characteristic values are presented in Table 1.

Table 1

Parameter	L	A	q	ρ_w	M_{sat}
Value	100	1	10	1000	20
Unit	μm	μm	μm	kg/ m^3	kA/m

Simulations were performed with one single cilium. The main purpose of either simulation was the investigation of the flow pattern, vortex structure and the flow rate. The magnetic engine is represented by an exterior harmonic magnetic field aligned in the x-direction. The salient features of one cilium harmonic 3D motion are illustrated in Figs. 2 and 3.

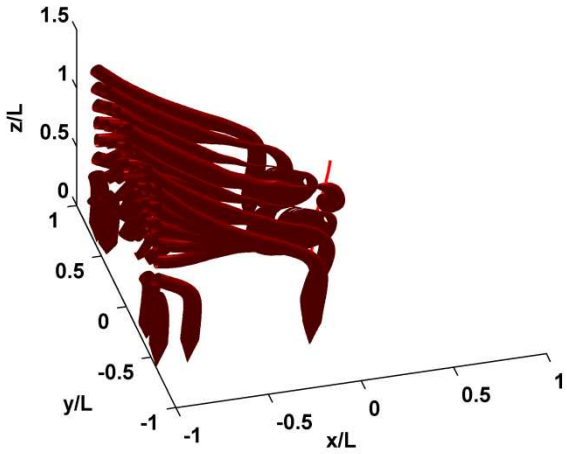

Figure 2. Streamline pattern at $\bar{t} = 0.30$. $B_x = 0.000625$ N/m·A, $E = 6 \cdot 10^6$ Pa and $f = 10$ Hz

The rigidity of the cilium ($E_B = E \cdot I$) affected by Young's elastic modulus (E), the induction and the frequency of magnetic field have great influence on the movement of the cilium and the pattern of streamlines in this special case of visco-elastic fluid. Figures 2 and 3 illustrate the particular case when $B_x = 0.000625$ N/m·A (Tesla), $E = 6 \cdot 10^6$ Pa and $f = 10$ Hz. We notice two large vortex stuctures nearby cilium similar those discovered in the

case of

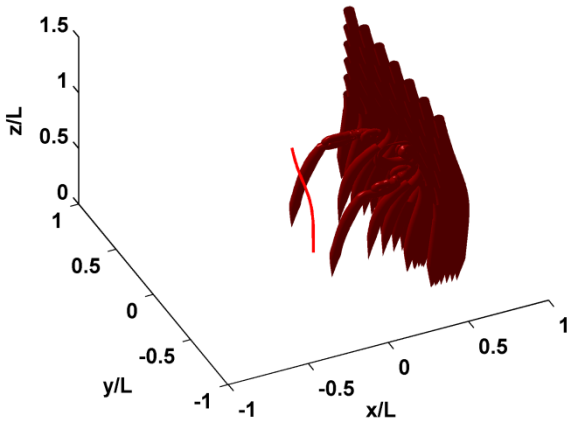

Figure 3. Streamline pattern at $\bar{t} = 1.07$. $B_x = 0.000625$ N/m·A, $E = 6 \cdot 10^6$ Pa and $f = 10$ Hz

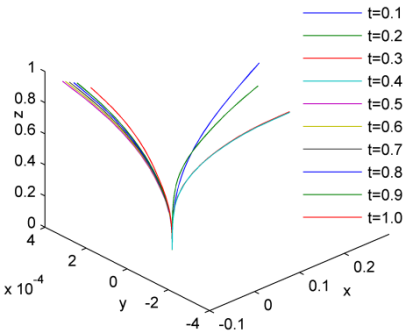

Figure 4. Cilium position at several instants over a cycle beat; $B_x = 0.0125$ N/m·A, $E = 3 \cdot 10^7$ Pa and $f = 10$ Hz - Case 1.

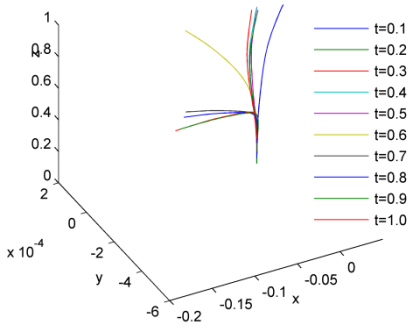

Figure 5. Cilium position at several instants over a cycle beat; $B_x = 0.0125$ N/m·A, $E = 3 \cdot 10^7$ Pa and $f = 25$ Hz – Case 2.

Newtonian fluids (Isvoranu et al., 2010). The major diference is that the vortices apear more frequently almost at each other cilium beat in the first stages of the movement. Later on, these structures disappear as illustrated in Fig. 2. Actually, the most important difference between cilium behavior in visco-elastic fluid as opposed to that in Newtonian fluid is represented by the vibrating component induced by the forcing magnetic field. In this

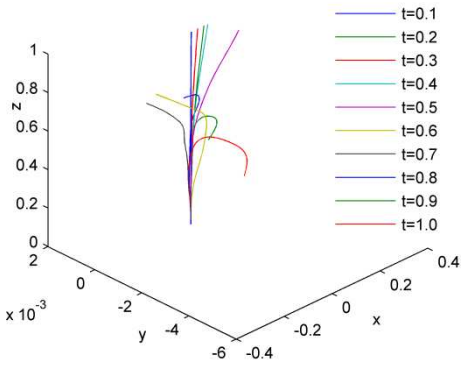

Figure 6. Cilium position at several instants over a cycle beat; $B_x = 0.00125$ N/m·A, $E = 6.6 \cdot 10^6$ Pa and $f = 15$ Hz – Case 3.

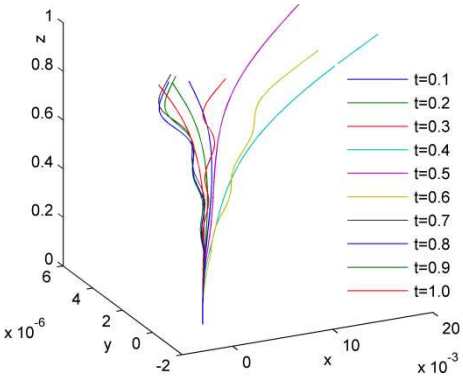

Figure 7. Cilium position at several instants over a cycle beat; $B_x = 0.00088$ N/m·A, $E = 6.6 \cdot 10^6$ Pa and $f = 15$ Hz – Case 4.

case, it is apparent an oscillatory movement similar to a vibrating chord. Resonant characteristics have been observed leading to loss of mechanical equilibrium. This can explain either the neccesity for extra rigidity or diminishing the active magnetic field induction. Figures 4-7 show snaphosts of cilium deformations during one cycle period for several external inputs. We notice the obvious influence of external field frecquency over cilium displacement in Fig. 4 and 5 while in Fig. 6 and 7 we observe the effect of

magnetic induction reduction. The augmented rigidity (Fig. 4-5) leads to a behavior similar to that found in the case of Newtonian fluid. The cilium oscillates in the fundamental mode. Lowering rigidity must be accompanied by lowering the active magnetic torque. Hence, shear rate diminishes and molecular viscosity increases over the cilium length. New behavior emerges and oscillates in higher modes like those illustrated in Fig. 6 and 7. Another interesting aspect is the mass flow rate transported by ciliary beat. The global net mass flow rate for the four cases analyzed is depicted in Table 2.

Table 2

Case	$\dot{m}$ [μg/s]
1	2.76
2	5.73
3	8.26
4	4.48

It seems that a good compromise between actuating force, frequency and rigidity is the key to high mass flow rate. The interesting thing is that considering the same parameters as in case 3 for a Newtonian fluid with $\mu_\infty = 0.001$ Pa·s, the global mass flow rate is of only $4.16 \cdot 10^{-3}$ μg/s, hence cilia beat in visco-elastic environment is much more productive.

7. Conclusion

The 3D motion of one cilium generates vortex dominated flow in certain circumstances. In the case of one-dimensional magnetic actuation the vortices are generally normal to the plane of the actuation. There is either a threshold of the magnetic torque that ensures mechanical stability or a specific rigidity. A significant energy saving is available in the case of visco-elastic environments.

References

Astarita G., Marruci G., 1977, Principles of non-newtonian fluid mechanics, Mc Graw Hill Book Co., New York.

Batchelor G.K., 1967. An Introduction to Fluid Mechanics. Cambridge University Press, UK.

Baltussen M., Onk P. and Toonder den J., 2010, Proceedings of the 2nd European Conference on Microfluidics - Microfluidics 2010 - Toulouse, December 8-10, 2010, μFLU'10, ISSN 2108-4718, ISBN 978-2-906831-85-8

Bird R.B., Hassager O., Armstrong R.C, and Curtiss C.F., 1987. Dynamics of Polymeric Liquids, Volume II, Kinetic Theory. Wiley & Sons, Inc., New York.

Chhabra R.P. and Richardson J.F.1999, Non-Newtonian Flow in the Process Industries. Fundamentals and Engineering Applications, Butterworth-Heinemann, Oxford.

Gueron, S., Liron, N., 1992. Ciliary motion modeling and dynamic multicilia interactions. Biophys. J., 63, 1045-1058.

Gueron, S., Levit-Gurevich, K., Liron, N., Blum, J.J., 1997. Cilia internal mechanism and metachronal coordination as the result of hydrodynamical coupling. Proc. Natl. Acad. Sci. USA, 94, pp 6001-6006, Applied Mathematics.

Gueron, S., Levit-Gurevich, K., 1998. Computation of the internal forces in cilia: Application to ciliary motion, the effects of viscosity and interactions. Biophys. J., 74, 1658-1676.

Gueron, S., Levit-Gurevich, 1999. Energetic considerations of ciliary beating and the advantage of metachronal coordination. Proc. Natl. Acad. Sci. USA, 96, no 2, pp 12240-12245, Applied Mathematics.

Gueron S, Levit-Gurevich K., 2001. The three-dimensional motion of slender filaments. Math. Meth. Appl. Sci., no. 24, pp 1577-1603.

Isvoranu, D., Ioan, D., Parvu, P., 2008. Numerical simulation of single artificial cilium magnetic driven motion in a semi-infinite domain. Proceedings of the 1st European Conference on Microfluidics - Microfluidics 2008 - Bologna, paper 226.

Isvoranu D., Ioan D., Danaila S., Parvu P., 2010. Numerical simulation of oscillating flow over a 3D Magnetic actuated array of cilia. Proceedings of the 2nd European Conference on Microfluidics - Microfluidics 2010 - Toulouse, December 8-10, 2010, µFLU'10, ISSN 2108-4718, ISBN 978-2-906831-85-8.

Jackson, J.D., 1974. Classical Electrodynamics John Wiley & Sons.

Malvern L. E., 1969. Introduction to the Mechanics of a Continuous Medium, Prentice Hall Englewood Cliffs, New Jersey.